

Viscoelastic transition in transonic flow focusing

A. Rubio ¹, F. J. Galindo-Rosales ², E. J. Vega ¹, J. M. Montanero ¹ and M. G. Cabezas ^{1,*}

¹*Depto. de Ingeniería Mecánica, Energética y de los Materiales and Instituto de Computación Científica Avanzada (ICCAEx), Universidad de Extremadura, E-06006 Badajoz, Spain*

²*CEFT, Departamento de Engenharia Química, Faculdade de Engenharia da Universidade do Porto, Rua Dr. Roberto Frias, 4200-465 Porto, Portugal*



(Received 21 October 2021; revised 25 November 2021; accepted 21 June 2022; published 14 July 2022)

We find and study the viscoelastic transition in transonic flow focusing when polymers of low molecular weights are dissolved in water at the appropriate concentration. This phenomenon is explained in terms of the coil-stretch transition of the polymers crossing the tapering meniscus, where the airstream produces very large strain rates. The resulting elastic stress stabilizes the flow, reducing the minimum liquid flow rate leading to jetting. As a consequence, we produce jets much thinner and longer than their Newtonian counterparts, which has important consequences at the technological level. We present a scaling analysis to show the role played by the polymer relaxation time and extensional viscosity in the viscoelastic transition.

DOI: [10.1103/PhysRevFluids.7.074201](https://doi.org/10.1103/PhysRevFluids.7.074201)

I. INTRODUCTION

In gaseous flow focusing [1], a liquid is injected at a constant flow rate through a feeding capillary located in front of an orifice [1] or inside a converging nozzle [2,3]. A coflowing gas stream is forced to cross the orifice/nozzle, which originates favorable pressure gradients and viscous stresses. The resulting forces sharpen the liquid meniscus attached to the feeding capillary and pull a thin jet from the meniscus tip. Straight and very thin jets can be produced when the outer gas stream is accelerated up to the sound speed and discharged into a low-pressure chamber (Fig. 1). For instance, water jets $\sim 1 \mu\text{m}$ in diameter and $\sim 100 \text{ km/h}$ in speed can be produced with this technique when they are powered by a transonic current of Helium [4,5].

Transonic flow focusing exhibits significant differences with respect to the original incompressible version of this technique [1]. In almost all the practical realizations, the jetting mode instability is originated in the tapering meniscus, while the convective-to-absolute instability transition [6] is not observed in the emitted jets [7]. The whipping (bending) instability [3] is suppressed because the jet is discharged into a low-pressure chamber. Besides, the scaling law for the jet diameter significantly differs from its counterpart in the incompressible mode [7].

Gaseous flow focusing has many important applications. Tiny droplets/capsules are formed with an acceptable degree of monodispersity from the breakup of the emitted simple/compound jets owing to the capillary instability. Microbubbles can also be ejected at the tip of a gaseous tapering meniscus when the outer (focusing, continuous) and inner (focused, dispersed) phases are exchanged. In all these cases, the size of the produced microfluidic entity is much smaller than that of any passage of the ejector owing to the action of the focusing current. Gaseous flow focusing has been used to produce, for instance, microparticles of complex structures [8,9] or to form stimuli-responsive microbubbles [10] for a wide range of applications in pharmacy and

*Corresponding author: mguadama@unex.es

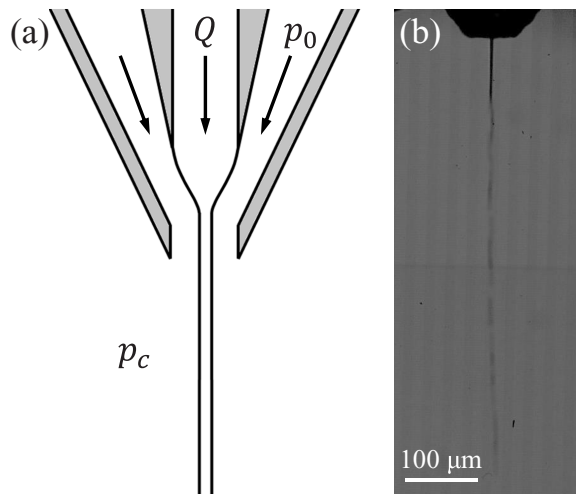


FIG. 1. (a) Sketch of the fluid configuration. (b) Water jet emitted at the flow rate $Q = 0.75$ ml/h driven by an air current with a stagnation pressure $p_0 = 2.5$ bar and discharged into a pressure chamber $p_c = 75$ mbar.

biomedicine. Transonic flow focusing has become one of the most successful ways to introduce samples in serial femtosecond crystallography (SFX) [4,5], which has revolutionized the molecular determination of complex biochemical species from proteins to viruses. The jet speed/diameter must be sufficiently large/low to fulfill the requirements of the high pulse rates used in SFX.

The flow focusing principle has also been applied to produce viscoelastic threads by replacing the Newtonian dispersed phase with a polymer solution [11,12]. In this case, the straining flow driven by the gaseous current increases the solution extensional viscosity, stabilizing the ejected thread until the solvent evaporation occurs. The focusing of viscoelastic solutions with gaseous currents [13,14] has been proposed for smooth printing and bioplotting [15], and to fabricate fibers with diameters ranging from a few microns down to hundreds of nanometers [16,17]. The flow focusing of weakly viscoelastic liquids in the transonic regime has not been analyzed yet.

Many dilute polymer solutions exhibit a practically constant viscosity (shear thinning behavior can be neglected) over a wide range of shear rates [18] so that the major polymer effects are the increase of the solution shear viscosity and elasticity. In ideal dilute solutions, neutral chains adopt a random coil configuration at equilibrium. The relaxation from the stretched to coil conformations consists of multiple processes. If the polymer relaxation time λ_p characterizing the slowest process is much larger than the rest of the spectrum, then the polymer solution elasticity can approximately be quantified by this parameter.

The response of the viscoelastic solution to a straining flow is generally characterized by the so-called extensional relaxation time λ_r , measured in filament thinning rheometers such as CaBER [19] and FiSER [20]. This parameter is usually linked to the polymer relaxation time λ_p , and increases with the polymer concentration of a dilute solution due to the hydrodynamic (flow-mediated) interaction among polymers.

It has been recognized for a long time that high-velocity gradients can cause the transition from a coil to a nearly completely stretched conformation of polymer chains [21]. For instance, and according to the Oldroyd-B and FENE-P models [22], the coil-stretch transition takes place in a uniaxial extensional flow if the stretching rate exceeds the threshold $\dot{\epsilon} = 1/(2\lambda_r)$ [23].

In some applications of gaseous flow focusing, such as SFX [4,5], the outer gas stream causes extremely high-velocity gradients in the tapering meniscus, which can induce the coil-stretch transition of polymer molecules even with low molecular weights (low relaxation times). In that case, the elastic stresses built up in the meniscus may substantially alter the flow stability and, therefore, the performance of the flow focusing technique. The major experimental finding of this work is

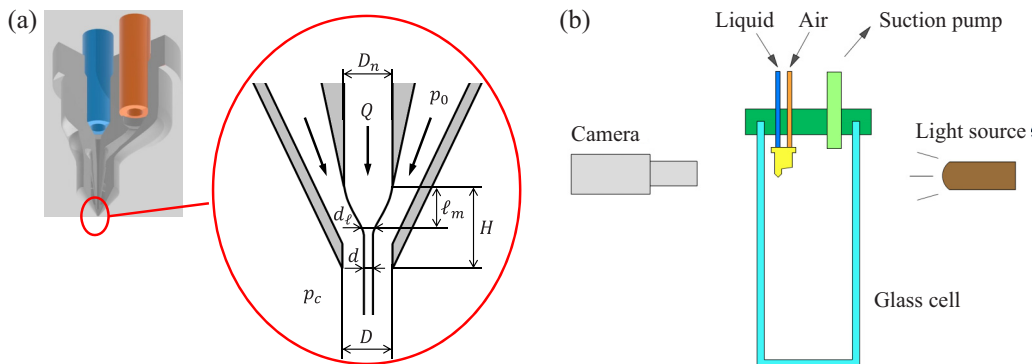


FIG. 2. Ejector (a) and elements of the experimental setup (b).

the existence of a viscoelastic transition in transonic flow focusing for small polymer molecular weights and appropriate concentrations. This transition leads to a substantial stabilization of the jetting regime, which reduces the minimum diameter of the emitted jet in one order of magnitude. This effect entails important advantages at the practical level.

II. MATERIALS AND METHODS

A. Experimental setup and procedure

The main elements of the experimental setup are shown in Fig. 2. A converging submillimeter nozzle was mounted onto the cap of a discharge glass cell. The nozzle tip consisted of a sharp inner needle of diameter $D_n = 75 \mu\text{m}$, located at a distance $H = 180 \mu\text{m}$ from the nozzle orifice exit of diameter $D = 75 \mu\text{m}$. We established a pressure $p_c = 75 \text{ mbar}$ inside the cell using a suction pump. The working liquid was injected at a constant flow rate Q through the inner needle with a syringe pump (Legato210, KD-Scientific). The focusing air stream was controlled by setting the stagnation pressure p_0 upstream with the pressure regulator of the compressed air line for positive pressures and throttling the flow from the atmosphere with a valve for the negative. We verified that the loss of stagnation pressure in the gas circuit was less than 3%.

Digital images of the liquid meniscus and jet were acquired at 2000 fps using a high-speed video camera (Fastcam Mini UX50) equipped with optical lenses (Optem Zoom 70XL) and a microscope objective (20X Optem) and white back-lighting. The images consisted of 1280×1024 pixels. The magnification was $3\times$, which resulted in $0.236 \mu\text{m}/\text{pixel}$. The camera could be displaced both horizontally and vertically using a triaxial translation stage. All the elements of the experimental setup were mounted on an optical table with a pneumatic antivibration isolation system to damp the vibrations coming from the building.

In steady jetting, a jet is emitted from the tip of the meniscus anchored to the inner needle [Fig. 2(a)]. We measure the jet diameter d at the nozzle exit with pixel resolution. The meniscus length ℓ_m is measured from the needle to the section at which the diameter has reached 80% of the total reduction ($D_n - d$). In other words, the meniscus length is the distance between the needle exit and the meniscus section with diameter $d_\ell = 0.2(D_n - d) + d$. To determine the minimum flow rate for steady jetting, we first set the upstream stagnation pressure and a sufficiently large liquid flow rate. Then, the latter was decreased in steps of 0.01 ml/h until the jetting regime became unstable. We repeated each experimental run three times to calculate the average value and the uncertainty, defined as the difference between the minimum and maximum values. We also determined the critical flow rate by increasing the flow rate until the jet became stable. We verified that the critical values obtained in this way differed in less than the experimental uncertainty. Therefore, hysteresis effects are negligible.

B. Nozzle fabrication

The nozzle [Fig. 2(a)] was printed using Nanoscribe Photonic Professional GT2 with the dip-in laser lithography (DiLL) configuration, dipping the $25\times$ objective into the IP-S resin droplet on an ITO coated glass substrate. We chose the shell and scaffolds writing strategy and produced a $20\ \mu\text{m}$ thickness shell delimiting the structure and an internal scaffold to stabilize the structure. The writing time was 35 h. The part was developed in ~ 25 ml of propylene glycol monomethyl ether acetate (PG-MEA) for 1 h and then cleaned in ethanol for 10 min. Then, unexposed resin inside the shell was cured for 60 min inside the UV Curing Chamber (XYZprinting).

C. Liquids

Aqueous polymeric solutions with different molecular weights and concentrations c were used as working liquids. The polymer was polyethylene oxide (Sigma Aldrich) with molecular weights $M_w = 100 \times 10^3$, 200×10^3 , 600×10^3 , 1000×10^3 , and 2000×10^3 g/mol. Hereafter, the acronym PEOX stands for a PEO aqueous solution with molecular weight of X (g/mol). Stock polymeric solutions were prepared by dissolving the polymers in deionized water with a magnetic stirrer for five days at low angular speeds to minimize mechanical degradation of the long polymer chains. These solutions are Boger fluids [18], i.e., they exhibit negligible shear thinning over a large range of shear rates, which allows analyzing the effects of elasticity separately. Using polymers with several molecular weights at different concentrations enabled us to vary the characteristic time λ_r systematically.

For the sake of comparison, we also conducted experiments with water-glycerol mixtures with the same Ohnesorge number $\text{Oh} = \eta(\rho\gamma D_n/2)^{-1/2}$ as some polymeric solutions. We will refer to these solutions as WX GY, where “X” and “Y” indicate the relative concentration in weight of water and glycerol, respectively.

D. Liquids characterization

The surface tension γ was measured with a Sigma 700 force tensiometer (Biolin Scientific, Espoo, Finland) equipped with a Du Nouÿ ring of 0.185 mm in thickness and 9.58 mm in diameter. This device was equipped with a spherical glass probe of $0.8836\ \text{cm}^3$ to measure the density ρ .

A stress-controlled rotational rheometer (Anton Paar MCR301) was used to obtain the steady shear viscosity η as a function of the shear rate $\dot{\gamma}$ of the polymeric solutions and the viscosity of the water-glycerol mixtures. We used a plate-plate geometry of 25 mm in radius, with a gap of $400\ \mu\text{m}$. The temperature within the fluid volume was set at $20\ ^\circ\text{C}$ and controlled by a Peltier element. Steady-state viscosity curves were obtained from 1 to $10^4\ \text{s}^{-1}$. At least three independent measurements were performed to ensure the reproducibility of the results. The range of shear rates providing reliable data was set for each sample between the limit of the rheometer sensitivity (low-shear rate limit) and the onset of elastic instabilities (high-shear rate limit). Figure 3 show the dependence of the solution shear viscosity η upon the shear rate $\dot{\gamma}$ for PEO100K [Fig. 3(a)] and PEO600K [Fig. 3(b)]. The shear thinning is negligible for all the cases but for the largest PEO100K concentration. We calculated the viscosity η as the mean value within the reliable measurement range. The results are shown in Fig. 3(c).

This work compares the behavior of flow focusing viscoelastic realizations and their corresponding Newtonian counterparts, i.e., those with the same value of the Ohnesorge number. Table I shows the measured properties and Ohnesorge number for the water/glycerol mixtures and the corresponding polymeric solutions. The values for the water/glycerol mixtures agree with those reported in the literature [24].

Rubio *et al.* [25] used a modified version of the capillary breakup extensional rheometer to measure the relaxation time λ_r of PEO100K dissolved in water at different concentrations. The results are shown in Fig. 4. This figure also shows the values for PEO600K measured in the present work with essentially the same procedure. The experimental data were fitted by power laws [26] to estimate the values of λ_r corresponding to the critical concentrations c_1^* defined in Sec. III. Those values are 20.3 and $14\ \mu\text{s}$ for PEO100K and PEO600K, respectively.

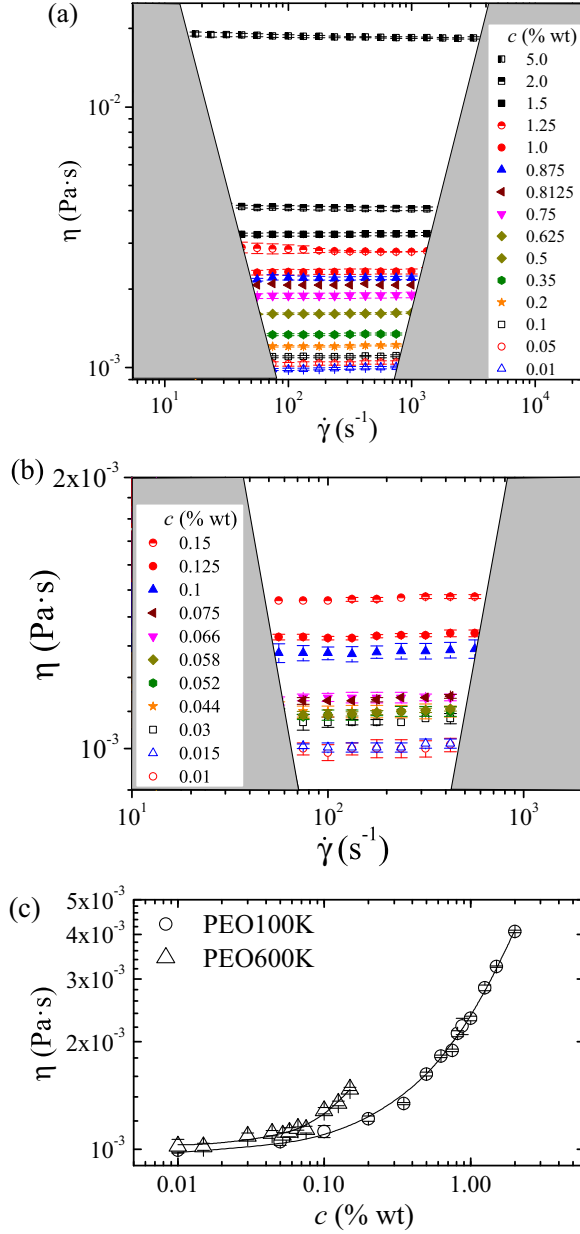


FIG. 3. Dependence of the solution shear viscosity η upon the shear rate $\dot{\gamma}$ at 20 °C for (a) PEO100K and (b) PEO600K solutions. (c) Mean shear viscosity dependence on the concentration. The solid lines are the fittings $\eta = (0.17c^2 + 1.23c + 0.97) \times 10^{-3}$ and $\eta = (12.94c^2 + 1.12c + 1.01) \times 10^{-3}$ for PEO100K and PEO600K respectively (with η and c measured in Pa s and %wt, respectively).

III. RESULTS AND DISCUSSION

Three types of menisci were found for the polymer solutions with the lowest molecular weights, PEO100K, PEO200K and PEO600K (Fig. 5). For small c and/or large Q , a “Newtonian-type meniscus” [Fig. 5(a1)] was observed. The shape of this meniscus was similar to that of

TABLE I. Density ρ , shear viscosity η , surface tension γ , and Ohnesorge number Oh for PEO solutions and the corresponding water/glycerol mixtures.

Liquid	ρ (kg/m ³)	η (mPa s)	γ (mN/m)	Oh
PEO100K 0.5%	1000	1.60	60.4	0.034
W80 G20	1043	1.77	66.5	0.035
PEO100K 0.875%	1000	2.21	60.5	0.046
W72 G28	1063	2.36	59.8	0.048
PEO100K 1.5%	1001	3.25	59.3	0.069
W60 G40	1090	3.28	69.0	0.062
PEO100K 2.0%	1002	4.41	59.6	0.093
W50 G50	1114	6.15	65.3	0.118

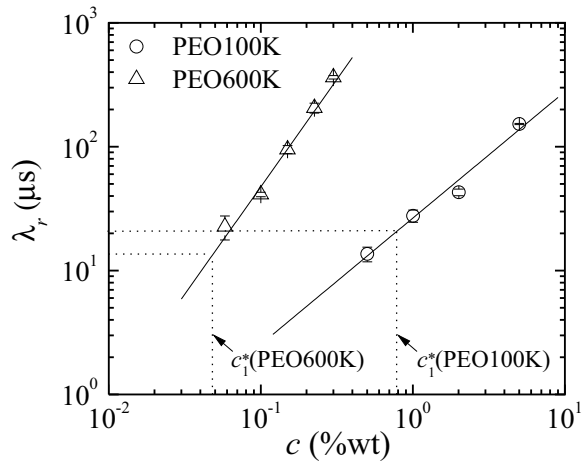


FIG. 4. Relaxation time λ_r of PEO100K and PEO600K dissolved in water at different concentrations. The solid lines are the fittings $\lambda_r = 26.18 c^{1.020}$ and $\lambda_r = 2707 c^{1.733}$ to the experimental results for PEO100K and PEO600K, respectively (with λ_r and c measured in μs and %wt, respectively). The dashed lines indicate the values of λ_r at the corresponding critical concentration c_1^* as defined in Sec. III.

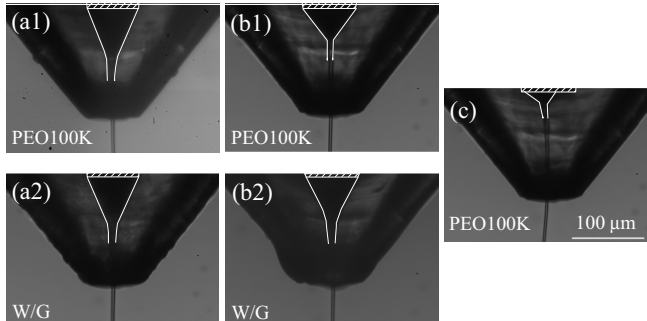


FIG. 5. Newtonian-type (a1) and viscoelastic (b1) menisci formed in the experiments with PEO100K for $\{c = 0.5\% \text{ wt}, Q = 1.57 \text{ ml/h}\}$ and $\{c = 0.875\% \text{ wt}, Q = 1.38 \text{ ml/h}\}$, respectively. Images (a2) and (b2) show the menisci of the water-glycerol mixture for the same Ohnesorge number and flow rate as those of the corresponding polymer solution. Image (c) shows the ejection mode following the pull-out instability for PEO100K, $c = 1.25\% \text{ wt}$, and $Q = 1 \text{ ml/h}$. All the experiments were conducted for $p_0 = 2.5 \text{ bar}$. The striped rectangle marks the needle tip, and the white lines the meniscus shape.

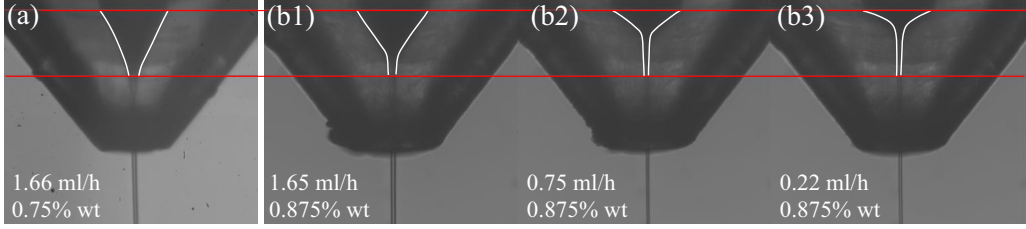


FIG. 6. Meniscus shape for PEO100K and $p_0 = 2.5$ bar. Images (a) and (b3) correspond to the minimum flow rate for those concentrations. The white lines mark the meniscus profile and the red lines are a guides to the eye.

water-glycerol with the same Ohnesorge number [Fig. 5(a2)]. For adequate values of c and Q , the meniscus significantly shrunk (the meniscus length decreased) [Fig. 5(b1)], while the triple contact line remained anchored to the needle edge. The shape of this “viscoelastic meniscus” noticeably differed from its water-glycerol counterpart [Fig. 5(b2)].

The viscoelastic effect was appreciable when the polymer concentration was slightly increased above the critical concentration c_1^* [Figs. 6(a) and 6(b1)]. For $c \gtrsim c_1^*$, the meniscus shrinkage considerably increased as Q decreased. In fact, the meniscus shape shown in Fig. 6(b3) has not been observed in any Newtonian flow focusing realization [7,27], regardless of the liquid viscosity and gas speed. Finally, the so-called pull-out effect was observed for large values of c and small values of Q . The contact line depinned from the capillary edge and moved upwards over the inner wall of the feeding capillary [Fig. 5(c)]. In this case, the jet was prone to whipping instability at the nozzle exit.

The Ohnesorge number of the viscoelastic meniscus in Fig. 5(b1) practically equals that of its water-glycerol counterpart [Fig. 5(b2)]. Figure 7 shows the meniscus length ℓ_m and the jet diameter d as a function of the flow rate Q for those two liquids. Steady jetting can be maintained for significant lower flow rates in the viscoelastic case. Although the jet diameter is similar for both fluids, the meniscus is significantly shorter in the viscoelastic case. The meniscus shrinkage must be attributed to elasticity because the Ohnesorge number is almost the same for the two liquids. Fluid particles undergo an intense extensional flow next to the meniscus interface dragged by the outer gas stream. In fact, the liquid velocity increases from values ~ 1 mm/s at the capillary exit up to the jet speed $v_j \sim 10$ m/s near the meniscus tip. This sharp increase takes place along distances $s \sim 100$ μ m. The resulting strain rate, $\dot{\epsilon} \simeq v_j/s \sim 10^5$ s $^{-1}$, is commensurate with the inverse of the extensional relaxation time λ_r^{-1} (see Fig. 4) for PEO100K, and the coil-stretch transition of the dissolved polymers occurs. The elastic stresses arising from that transition collaborate with those exerted by the outer flow in pushing the liquid throughout the meniscus-jet region. The resulting extra acceleration explains the meniscus shrinkage. When the flow rate is decreased, the jet speed near the meniscus tip increases [7], the meniscus length decreases (Fig. 7), and, therefore, the strain rate field in the meniscus increases. This effect enhances the building-up of the elastic stress, which explains why the meniscus shrinkage sharply increases as Q decreases.

Finally, if the polymer concentration is further increased, then the large tensile stress arising in the meniscus makes it detach from the needle edge and climb over the inner needle wall (the pull-out effect [28–30]). In this case, the final position of the triple contact line is essentially determined by the balance between the tensile force originating from the Poiseuille-like flow in the needle, and that exerted by the emitted jet. This pull-out phenomenon has frequently been observed in fiber spinning [28–30].

The transition from a quasi-Newtonian to viscoelastic behavior described above considerably alters the stability map of transonic flow focusing. Figure 8(a) shows the ejection modes adopted by our configuration for different concentrations of PEO100K. The smallness of the error bars shows the high degree of experimental reproducibility. For $c < c_1^*$ ($c_1^* \simeq 0.78\%$ wt), the minimum flow

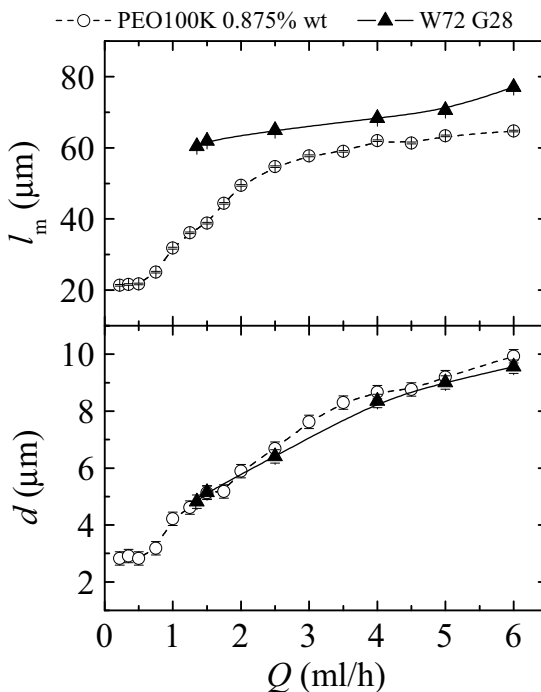


FIG. 7. Meniscus length ℓ_m and jet diameter d as a function of the flow rate Q for PEO100K at $c = 0.875\%$ wt (circles) and the water-glycerol mixture with the same Oh (triangles). The lowest flow rate in each case shows the corresponding stability limit. The experiments were conducted for $p_0 = 2.5$ bar.

rate Q_{\min} leading to the jetting regime slightly increases with c . The same trend is observed for the water/glycerine (Newtonian) mixtures with the same Ohnesorge numbers. Therefore, this effect can be attributed to the increase of the solution viscosity. At the critical concentration $c = c_1^*$, Q_{\min} plunges. The critical flow rate remains almost constant in the interval $c_1^* < c < c_2^*$ ($c_2^* \simeq 1.13\%$ wt), and is around six times smaller than the value $Q_{\min} = 1.4$ ml/h measured for water-glycerol with a similar Ohnesorge number. The sharp decrease of Q_{\min} at $c = c_1^*$ is caused by the coil-stretch transition also responsible for the meniscus shrinkage. As mentioned above, this transition triggers the polymeric force, which collaborates with the outer stream force in pushing the liquid through the critical meniscus-jet region. This effect helps the fluid to overcome the resistant viscous and surface tension forces emerging in that region. Finally, Q_{\min} sharply increases at $c = c_2^*$. This effect is associated with the pull-out instability described above.

The results shown above indicate that, when PEO polymers of low molecular weights are dissolved in water at the appropriate concentration, the flow rate can be reduced in around one order of magnitude while keeping the steady jetting regime running. This reduction has important practical consequences because it allows one to produce much thinner jets than their Newtonian counterparts [see Figs. 7 and 8(b)]. For instance, the minimum jet diameter d_{\min} (d at $Q = Q_{\min}$) of water becomes 2–3 times smaller when PEO100K molecules are dissolved at the concentration $c = 0.8125\%$ wt (Fig. 9). This minimum jet diameter is smaller than that expected from the Newtonian scaling law $d_{\min} \sim Q_{\min}^{0.808}$ [7], probably due to the increase of the extensional viscosity associated with the polymer stretching.

Interestingly, the jet's length drastically increased at $c = 0.75\%$ wt, i.e., the concentration just below the critical one c_1^* . In fact, we could not observe the breakage of viscoelastic jets for concentrations larger than that value (Fig. 9). This result indicates that the viscoelastic transition in the tapering meniscus and in the emitted jet occurs at practically the same concentrations.

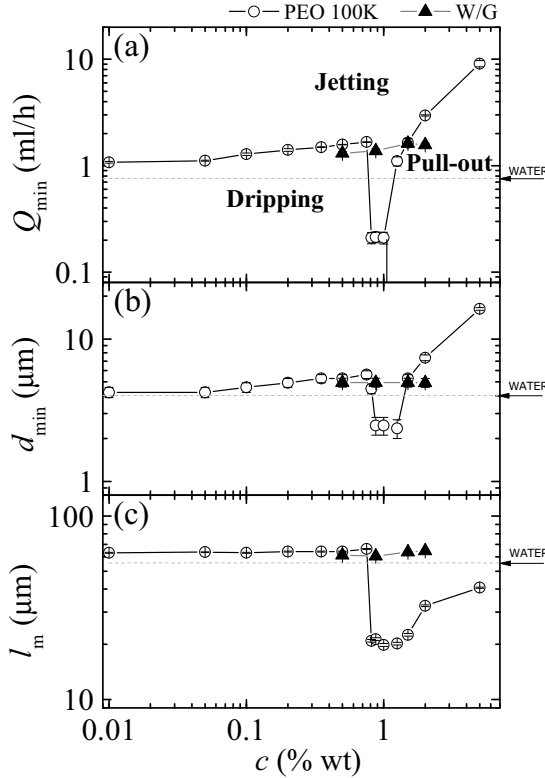


FIG. 8. (a) Ejection modes adopted by flow focusing. The symbols indicate the minimum flow rates leading to the jetting regime. (b) Jet diameter d_{\min} at the minimum flow rate. The circles correspond to the viscoelastic solutions and the triangles to the water-glycerol mixtures with the same Ohnesorge number as the polymer solution of concentration c . The solid lines are guides to the eye. The horizontal dashed line indicates the minimum flow rate and diameter for water. The experiments were conducted for $p_0 = 2.5$ bar.

We analyze the effect of the outer stream stagnation pressure p_0 on the viscoelastic transition in Fig. 10. The critical concentration c_1^* hardly depends on p_0 . This can be explained as follows. The transonic gas flow is choked for all the stagnation pressures applied in the experiments, which implies that the viscous driving force exerted by the outer stream on the liquid meniscus remains practically constant when p_0 is varied [7]. Therefore, the strain rate field induced by the outer stream in the liquid meniscus slightly depends on p_0 , which means that the coil-stretch transition comes into play practically at the same polymer concentration c_1^* . As explained above, the pull-out instability results from the imbalance between the normal stresses at the inlet and outlet sections of the meniscus. The variation of p_0 does affect the hydrostatic pressure distribution along the meniscus axis. This explains why the critical concentration c_2^* increases for small stagnation pressures, which implies that the optimum interval of c leading to the flow stabilization increases as p_0 decreases.

Results similar to those of PEO100K have also been obtained for other low-molecular-weight polymers, such as PEO200K and PEO600K (Fig. 11). The curves $Q_{\min}(c)$ and $d_{\min}(c)$ shift towards lower concentrations when the molecular weight is increased. This occurs because the extensional relaxation time λ_r increases with the molecular weight, and, therefore, it exceeds the threshold leading to the coil-stretch transition for lower concentrations. In fact, the values of λ_r for PEO100K and PEO600K at their respective critical concentrations c_1^* are commensurate with each other (see Fig. 4). The decrease in Q_{\min} at the critical concentration c_1^* becomes smaller as the molecular

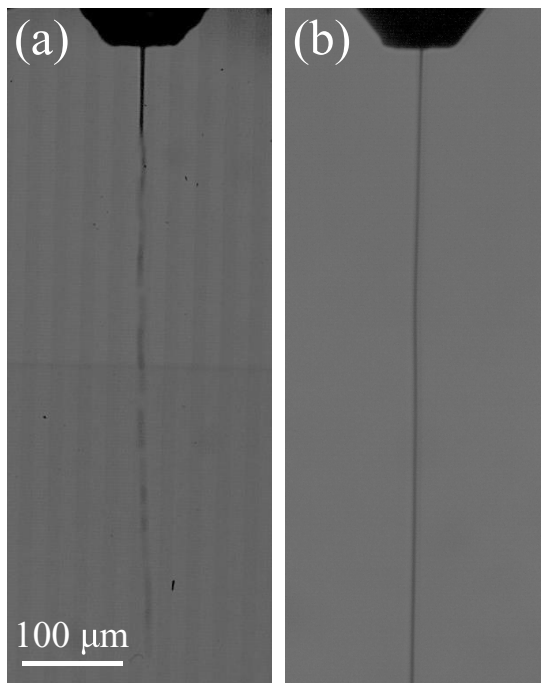


FIG. 9. Comparison of the jets emitted at the corresponding minimum flow rate: (a) water at $Q = 0.75$ ml/h and (b) PEO100K at $c = 0.8125\%$ and $Q = 0.2$ ml/h. The experiments were conducted for $p_0 = 2.5$ bar.

weight increases. Our experiments for molecular weights greater than 600K (i.e., for PEO1M and PEO2M) showed the pull-out effect at all the polymer concentrations.

As mentioned above, the viscoelastic transition takes place when the strain rate in the tapering meniscus exceeds the critical value leading to the coil-stretch transition. For this reason, we define the Weissenberg number $Wi = \lambda_r \langle \dot{\epsilon} \rangle$, where $\langle \dot{\epsilon} \rangle = v_\ell / \ell_m$ is the mean strain rate along the meniscus axis. Here, v_ℓ is the liquid velocity at the end of the meniscus and ℓ_m the meniscus length, as mentioned above.

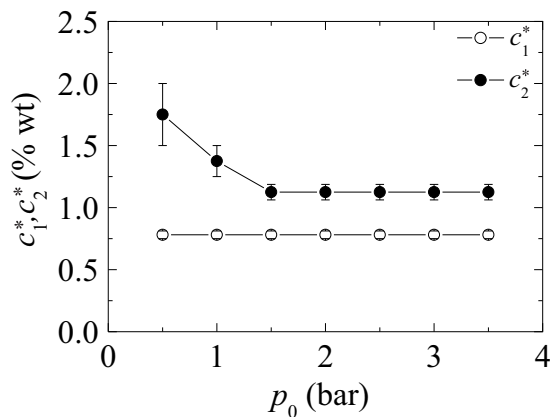


FIG. 10. Critical concentrations c_1^* and c_2^* as a function of the outer stream stagnation pressure p_0 for PEO100K.

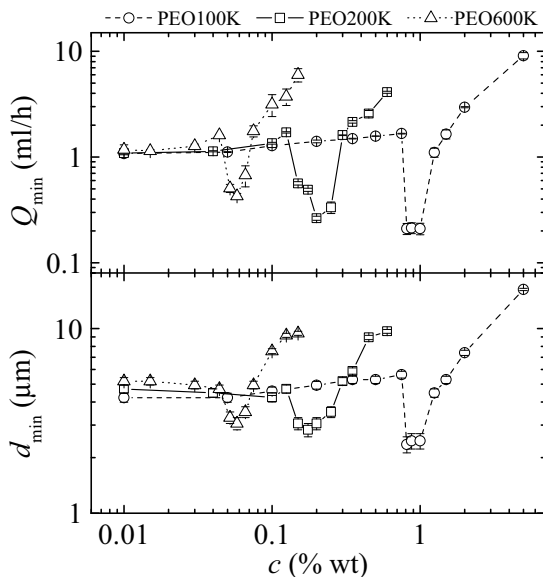


FIG. 11. Minimum flow rates leading to the jetting regime and the corresponding diameters for polymer solutions with different molecular weights.

In the low-viscosity Newtonian case, the flow instability is believed to be caused by the growth of recirculation cells in the tapering meniscus for small flow rates [27,31]. This mechanism is controlled by the liquid shear viscosity. For this reason, the minimum flow rate Q_{\min} scales as the characteristic flow rate $Q_D = D_n \eta / \rho$ [27,31,32], defined in terms of the shear viscosity η . In the high-viscosity Newtonian case, viscous stresses “arrange” the streamlines and “direct” the flow in the meniscus tip. The recirculation cells disappear, and the instability is determined by the balance between the pressure drop and surface tension [27]. Then, the minimum flow rate scales as $Q_v = D_n^2 \gamma / \eta_e$. The inclusion of the Newtonian extensional viscosity $\eta_e = 3\eta$ (instead of η) in the definition of Q_v does not significantly change the scaling of Montanero *et al.* [27] because it only introduces a constant factor. The viscosity of the water-glycerol mixtures ranges from 1.8 to 6.2 mPa s, which corresponds to a moderately low viscosity regime. As expected, Q_{\min} is of the order of Q_D for these liquids.

In this work, we propose the natural extension of the above scaling for Newtonian liquids to the weakly viscoelastic case. For $c < c_1^*$, the tapering meniscus can be regarded as a Newtonian low-viscosity meniscus. Therefore, the minimum flow rate is expected to scale as Q_D [31,32]. For $c > c_1^*$, the stretching of the polymer chains drastically increases the solution extensional viscosity η_e , and the minimum flow rate is expected to scale as Q_v . When the coil-stretch transition takes place, the scale of the extensional viscosity can be calculated as $\eta_e = 3\lambda_r \gamma / d_\ell$ [23], where d_ℓ is the diameter at the meniscus end. The above scaling leads to the following definition of the dimensionless minimum flow rate:

$$\Phi = \begin{cases} \text{Re} = Q_{\min}/Q_D & \text{for } c < c_1^* \\ \text{Ca} = Q_{\min}/Q_v & \text{for } c > c_1^* \end{cases} \quad (1)$$

The dimensionless number Φ reduces to the Reynolds number based on the shear viscosity η for $c < c_1^*$ and the capillary number based on the extensional viscosity η_e beyond the viscoelastic transition.

Figure 12 shows $\Phi(\text{Wi})$ for the two polymers with considerably different molecular weights, PEO100K and PEO600K. The two curves practically overlap, which shows the validity of our scaling. The viscoelastic transition takes place around $\text{Wi} = 1/2$, the critical value for the coil-stretch

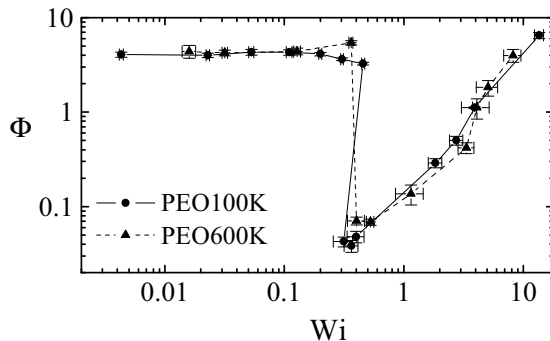


FIG. 12. $\Phi(Wi)$ for PEO100K and PEO600K. Experiments were conducted for $p_0 = 2.5$ bar.

transition in a simple extensional flow [23,33]. This result confirms that the sharp decrease of the minimum flow rate and, consequently, the minimum jet diameter is caused by the coil-stretch transition triggered by the large strain rate arising in the flow focusing meniscus. The Reynolds number (Φ for $c < c_1^*$) takes an approximately constant value, which indicates that the minimum flow rate scales as the viscosity. The values of the Reynolds number are similar to those of Newtonian low-viscosity menisci [27]. The capillary number (Φ for $c > c_1^*$) takes values of the same order of magnitude as that of the Newtonian high-viscosity case [27]. The experimental realizations for large Wi are affected by the pull-out instability. In this case, the triple contact line detaches from the capillary edge, and the balance between the spinning force and the normal stress in the feeding capillary determines the new position of the meniscus inside the capillary [30] (see Fig. 4 in Ref. [13]). We do not have a definitive explanation of the power law followed by $\Phi(Wi)$ when the triple contact line is detached.

IV. CONCLUSIONS

We have analyzed the viscoelastic transition occurring in transonic flow focusing when polymers of low molecular weights are added to water at an adequate concentration. This phenomenon is caused by the coil-stretch transition of polymers in the tapering meniscus. Despite the smallness of their relaxation time, the large strain rate produced by the transonic outer stream manages to stretch the polymers. The elastic stresses built up in the meniscus shrink it and stabilize the flow, which reduces the minimum flow rate for which the jetting regime is obtained. The phenomenon described above is reproducible and robust. It appears for a wide range of gas stagnation pressures and polymers with different molecular weights. When working in the appropriate parameter window, the flow rate and the jet diameter in transonic flow focusing can be reduced in one order of magnitude.

Our scaling analysis for the minimum flow rate reveals the role played by the polymer relaxation time and extensional viscosity in the viscoelastic transition. This transition takes place for Weissenberg numbers around 0.5. The Reynolds number takes values of order unity for subcritical realizations ($c < c_1^*$), as occurs in the Newtonian low-viscosity case [31,32]. For supercritical polymer concentrations ($c > c_1^*$), the capillary number, defined in terms of the polymer extensional viscosity, is a function of the Weissenberg number. The smaller values taken by the capillary number are similar to those of the Newtonian high-viscosity case [27].

The discontinuity seen in Fig. 12 is inherent to the viscoelastic transition taking place at $c = c_1^*$ and cannot be smoothed by an alternative scaling. In fact, the coil-stretch transition alters the microscopic structure of the focused liquid, and, therefore, the fluid behavior is expected to be fundamentally different beyond the critical concentration.

A natural question is whether polymers may suffer some kind of degradation or entanglement during the liquid ejection for the critical conditions. In principle, this possibility could be tested

by conducting extensional rheometry after the liquid ejection. However, measuring extensional relaxation times below $50 \mu\text{s}$ is very challenging [25]. The problem becomes even more complicated when one has to collect the sample after the ejection because contamination and/or evaporation would make the measurement unreliable.

The results presented in this paper may be of interest for researchers working in several fields, such as microfluidics, pharmacy, biotechnology, and crystallography. In essence, we have found a small parameter window within which much thinner jets can be produced with flow focusing. In our experiments, the water jet diameter was reduced in one order of magnitude without substantially changing its chemical composition (the polymer molecular weight and concentration were very small), which enhances the applications of flow focusing, particularly in highly demanding and important applications such as SFX.

ACKNOWLEDGMENTS

Support from the Spanish Ministry of Science and Education (Grant No. PID2019-108278RB-C32/AEI/10.13039/501100011033) and Gobierno de Extremadura (Grant No. GR21091) is gratefully acknowledged. F.J.G.R. also acknowledges the financial support by FEDER funds through COMPETE2020-Programa Operacional Competitividade e Internacionalização (POCI); Fundação para a Ciência e Tecnologia (FCT) and Ministério da Ciência, Tecnologia e Ensino Superior (MCTES) through national funds (PIDDAC) through Projects No. PTDC/EME-APL/30765/2017-POCI-01-0145-FEDER-030765 and No. UIDB/00532/2020, and the program Stimulus of Scientific Employment, Individual Support-2020.03203.CEECIND.

-
- [1] A. M. Gañán-Calvo, Generation of Steady Liquid Microthreads and Micron-Sized Monodisperse Sprays in Gas Streams, *Phys. Rev. Lett.* **80**, 285 (1998).
 - [2] D. P. DePonte, U. Weierstall, K. Schmidt, J. Warner, D. Starodub, J. C. H. Spence, and R. B. Doak, Gas dynamic virtual nozzle for generation of microscopic droplet streams, *J. Phys. D: Appl. Phys.* **41**, 195505 (2008).
 - [3] A. J. Acero, C. Ferrera, J. M. Montanero, and A. M. Gañán-Calvo, Focusing liquid microjets with nozzles, *J. Micromech. Microeng.* **22**, 065011 (2012).
 - [4] H. N. Chapman *et al.*, Femtosecond X-ray protein nanocrystallography, *Nature (London)* **470**, 73 (2011).
 - [5] S. Boutet *et al.*, High-resolution protein structure determination by serial femtosecond crystallography, *Science* **337**, 362 (2012).
 - [6] P. Huerre and P. A. Monkewitz, Local and global instabilities in spatially developing flows, *Annu. Rev. Fluid Mech.* **22**, 473 (1990).
 - [7] M. Rubio, A. Rubio, M. G. Cabezas, M. A. Herrada, A. M. Gañán-Calvo, and J. M. Montanero, Transonic flow focusing: Stability analysis and jet diameter, *Int. J. Multiphase Flow* **142**, 103720 (2021).
 - [8] A. M. Gañán-Calvo, R. González-Prieto, P. Riesco-Chueca, M. A. Herrada, and M. Flores-Mosquera, Focusing capillary jets close to the continuum limit, *Nat. Phys.* **3**, 737 (2007).
 - [9] A. M. Gañán-Calvo, J. M. Montanero, L. Martín-Banderas, and M. Flores-Mosquera, Building functional materials for health care and pharmacy from microfluidic principles and Flow Focusing, *Adv. Drug Deliv. Rev.* **65**, 1447 (2013).
 - [10] T. Si, G. B. Li, Q. Wu, an Z. Q. Zhu, X. S. Luo, and R. X. Xu, Optical droplet vaporization of nanoparticle-loaded stimuli-responsive microbubbles, *Appl. Phys. Lett.* **108**, 111109 (2016).
 - [11] K. V. Edmond, A. B. Schofield, M. Marquez, J. P. Rothstein, and A. D. Dinsmore, Stable jets of viscoelastic fluids and self-assembled cylindrical capsules by hydrodynamic focusing, *Langmuir* **22**, 9052 (2006).
 - [12] L. Derzsi, M. Kasprzyk, J. P. Plog, and P. Garstecki, Flow focusing with viscoelastic liquids, *Phys. Fluids* **25**, 092001 (2013).

- [13] A. Ponce-Torres, J. M. Montanero, E. J. Vega, and A. M. Gañán-Calvo, The production of viscoelastic capillary jets with gaseous flow focusing, *J. Non-Newtonian Fluid Mech.* **229**, 8 (2016).
- [14] E. Hofmann, K. Krüger, C. Haynl, T. Scheibel, M. Trebbin, and S. Förster, Microfluidic nozzle device for ultrafine fiber solution blow spinning with precise diameter control, *Lab Chip* **18**, 2225 (2018).
- [15] A. Ponce-Torres, E. J. Vega, A. A. Castrejón-Pita, and J. M. Montanero, Smooth printing of viscoelastic microfilms with a flow focusing ejector, *J. Non-Newtonian Fluid Mech.* **249**, 1 (2017).
- [16] A. Ponce-Torres, E. Ortega, M. Rubio, A. Rubio, E. J. Vega, and J. M. Montanero, Gaseous flow focusing for spinning micro and nanofibers, *Polymer* **178**, 121623 (2019).
- [17] R. Vasireddi, J. Kruse, M. Vakili, S. Kulkarni, T. F. Keller, D. C. F. Monteiro, and M. Trebbi, Solution blow spinning of polymer/nanocomposite micro-/nanofibers with tunable diameters and morphologies using a gas dynamic virtual nozzle, *Sci. Rep.* **9**, 14297 (2019).
- [18] D. F. James, Boger fluids, *Annu. Rev. Fluid Mech.* **41**, 129 (2009).
- [19] G. H. McKinley and A. Tripathi, How to extract the Newtonian viscosity from capillary breakup measurements in a filament rheometer, *J. Rheol.* **44**, 653 (2000).
- [20] S. L. Anna and G. H. McKinley, Elasto-capillary thinning and breakup of model elastic liquids, *J. Rheol.* **45**, 115 (2001).
- [21] A. Peterlin, Hydrodynamics of linear macromolecules, *Pure Appl. Chem.* **12**, 563 (1966).
- [22] R. B. Bird, R. C. Armstrong, and O. Hassager, *Dynamics of Polymeric Liquids Volume I: Fluid Mechanics; Volume II: Kinetic Theory* (Wiley, New York, 1987).
- [23] J. Eggers and E. Villermaux, Physics of liquid jets, *Rep. Prog. Phys.* **71**, 036601 (2008).
- [24] K. Takamura, H. Fischer, and N. R. Morrow, Physical properties of aqueous glycerol solutions, *J. Pet. Sci. Eng.* **98–99**, 50 (2012).
- [25] M. Rubio, A. Ponce-Torres, E. J. Vega, and J. M. Montanero, Experimental analysis of the extensional flow of very weakly viscoelastic polymer solutions, *Materials* **13**, 192 (2020).
- [26] P. E. Rouse, A theory of the linear viscoelastic properties of dilute solutions of coiling polymers, *J. Chem. Phys.* **21**, 1272 (1953).
- [27] J. M. Montanero, N. Rebollo-Muñoz, M. A. Herrada, and A. M. Gañán-Calvo, Global stability of the focusing effect of fluid jet flows, *Phys. Rev. E* **83**, 036309 (2011).
- [28] T. Sridhar and R. K. Gupta, Fluid detachment and slip in extensional flows, *J. Non-Newtonian Fluid Mech.* **30**, 285 (1988).
- [29] M. J. H. Bulters and H. E. H. Meijer, Analogy between the modelling of pullout in solution spinning and the prediction of the vortex size in contraction flows, *J. Non-Newtonian Fluid Mech.* **38**, 43 (1990).
- [30] C. van der Walt, M. A. Hulsen, A. C. B. Bogaerds, H. E. H. Meijer, and M. J. H. Bulters, Stability of fiber spinning under filament pull-out conditions, *J. Non-Newtonian Fluid Mech.* **175–176**, 25 (2012).
- [31] M. A. Herrada, A. M. Gañán-Calvo, A. Ojeda-Monge, B. Bluth, and P. Riesco-Chueca, Liquid flow focused by a gas: Jetting, dripping, and recirculation, *Phys. Rev. E* **78**, 036323 (2008).
- [32] T. Si, F. Li, X.-Y. Yin, and X.-Z. Yin, Modes in flow focusing and instability of coaxial liquid-gas jets, *J. Fluid Mech.* **629**, 1 (2009).
- [33] V. M. Entov and E. J. Hinch, Effect of a spectrum of relaxation times on the capillary thinning of a filament of elastic liquid, *J. Non-Newtonian Fluid Mech.* **72**, 31 (1997).